THE ASTROPHYSICAL JOURNAL, 555:850–854, 2001 July 10

MEASURING THE MAGNETIC FIELD STRENGTH IN L1498 WITH ZEEMAN-SPLITTING OBSERVATIONS OF CCS

S. M. LEVIN, W. D. LANGER, T. VELUSAMY, AND T. B. H. KUIPER
Jet Propulsion Laboratory, California Institute of Technology, m/s 169-506, Pasadena, CA 91109; steven.levin@jpl.nasa.gov
AND
R. M. CRUTCHER
Department of Astronomy, University of Illinois at Urbana-Champaign
Received 2000 December 4; accepted 2001 March 20

ABSTRACT

We have measured the Zeeman splitting of the CCS $J_N = 3_2$–2_1 line at 33 GHz toward L1498, a dense preprotostellar core, in an effort to measure the line-of-sight component of its magnetic field. With approximately 35 hr of data on source (70 hr total) in good weather, the data suggest a line-of-sight component of the magnetic field in L1498 of 48 ± 31 μG, yielding an upper limit of $B_{\rm los} < 100$ μG at the 95% confidence level. This upper limit provides some constraints on models. Our results show that the technique we have adopted to measure CCS Zeeman splitting holds great promise for determining magnetic field strengths in cloud cores using lower-frequency transitions, in particular the CCS $J_N = 1_0$–0_0 line at 11 GHz. At this transition, the frequency splitting per gauss is 3 times that at 33 GHz, the brightness temperature is comparable to the 3_2–2_1 line, and receiver systems can be made more sensitive.

Subject headings: ISM: clouds — ISM: magnetic fields — ISM: molecules — magnetic fields — stars: formation

1. INTRODUCTION

Magnetic fields play an important role, perhaps second only to that of gravity, in the development of dense, cold, protostar-forming cores in molecular clouds, but we have very little direct information about the strength of the magnetic field within the cores themselves. Zeeman splitting in OH and H I lines has been used to deduce the field strength in molecular and atomic clouds (see Crutcher & Troland 2000 and references therein), but the comparatively large beam sizes and the ubiquity of OH and H I make it extremely difficult to draw conclusions about the magnetic field in the smaller dense structures, which are the most important for understanding protostar formation. Instead, we need a molecule with large enough Zeeman splitting to trace high-density protostellar cores. Ordering by splitting coefficient, the best possible candidates are SO, CCS, and CN (Fiebig 1990). The 113 GHz lines of CN have recently been used to measure field strength (Crutcher 1999), but CN is seen mainly in hotter, denser regions ($n > 10^6$ cm^{-3}). Unfortunately, SO is not widespread and even when present has very weak lines in the dense protostellar cores. In contrast, CCS is potentially a good probe of magnetic fields, because it is found in the dense cores at H_2 densities of 10^4–10^5 cm^{-3} and has a reasonable Zeeman-splitting coefficient. Further, it has several transitions accessible at cm wavelengths, where the Doppler broadening is less and the required excitation temperature is lower than for CN, making the Zeeman effect in principle easier to measure.

We have undertaken a program of measuring the CCS Zeeman splitting in preprotostellar cores. Taking advantage of the unique capabilities of NASA's Deep Space Network (DSN) antennas, we have observed the 33.751 GHz $J_N = 3_2$–2_1 transition of CCS with a 34 m diameter radio telescope and an ultralow-noise dual-polarization maser receiver. We chose to study L1498, a dark cloud in Taurus, because it has a cold, dense core of a few solar masses in a precollapse state, with strong, narrow, CCS line emission (Kuiper, Langer, & Velusamy 1996; Willacy, Langer, & Velusamy 1998). Furthermore, the velocity field in L1498 is very well known from these previous high-quality CCS maps, so that we are able to find a location (the peak of the NH_3 and continuum emission) where the velocity gradient is close to zero, reducing the impact of pointing differences between left-circular polarization (LCP) and right-circular polarization (RCP; see Fig. 1).

After 70 hr of observing L1498 in good conditions, we have a formal result for the line-of-sight field, $B_{\rm los} = 48 \pm 31$ μG. Our work shows that Zeeman splitting of CCS has great promise for measuring the magnetic field in preprotostellar cloud cores, but the approach would work better at lower frequencies, where the splitting is larger and the system temperature can be lower. For example, the 11 GHz transition of CCS has a splitting of 21 km s^{-1} G^{-1}, compared to 7 km s^{-1} G^{-1} for the 33 GHz transition, and the atmospheric and receiver contributions will be lower.

2. EXPERIMENTAL CONCEPT

The concept of our measurement is simple. By measuring the RCP and LCP components of the 33.751 GHz $J_N = 3_2$–2_1 transition, we determine the frequency shift due to Zeeman splitting and hence the ordered component of the magnetic field in the core parallel to the line of sight. In practice, the expected frequency shift is small ($\sim$40 Hz) compared to the line width (12 kHz) at 33 GHz, and the velocity structure of L1498 can produce a Doppler variation larger than the shift to be measured (Kuiper et al. 1996). Therefore, systematic errors are extremely important, and we have spent substantial effort understanding and reducing systematic effects. Because we are only interested in the frequency shift, the measurement is insensitive to gain or offset variations that are not sharply frequency-dependent, involving significant variation on scales of the 12 kHz line width. However, any effect that introduces a frequency-dependent difference between the RCP and LCP spectra can potentially bias our measurement. Potential sources of systematic error include frequency-dependent

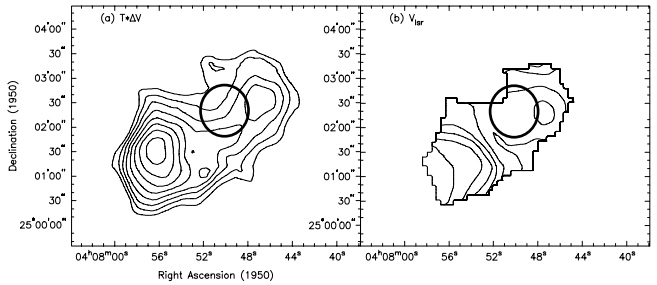

FIG. 1.—The CCS $J_N = 2_1$–1_0 emission at 22 GHz in L1498, from the data in Kuiper et al. (1996). (*a*) Integrated intensity. The ellipse marks the location and beam size for the measurements reported here. The first contour and contour interval are 0.03 K km s^{-1}. (*b*) Mean v_{LSR}. The first (southeast) and last (northwest) contours are 7.810 and 7.870 km s^{-1}, respectively. Contour interval is 0.010 km s^{-1}. The position observed for these measurements (*ellipse*) was chosen to have minimal velocity gradient.

differences in the gain of the RCP and LCP channels and polarization-dependent variations in the antenna beam pattern that correlate with velocity variations in the source field. We employed a number of approaches to reduce such systematic errors.

1. Subtracting off-source from on-source observations mitigates the effects of $1/f$ variation in the receiver noise and removes differences between RCP and LCP that are stable on the 10 minute timescale of integration and are not associated with antenna pointing.
2. The RCP and LCP spectra are taken simultaneously (rather than switching or using a polarization wheel), eliminating the effects of a wide range of possible temporal variations.
3. In the receiver back end, the RCP and LCP channels are mixed to slightly (20 MHz) different frequencies, filtered, and combined into a single passband, so that much of the signal path is shared.
4. We use 19 Hz spectral resolution per channel, allowing identification and elimination of any possibly polarized radio frequency interference (RFI).
5. The antenna pointing is measured separately with point sources to look for differences between LCP and RCP.
6. For each 10 minute observation, we fit a linear baseline and Gaussian line shape separately to each polarization. This removes any systematic effects that are not sharply frequency-dependent, and the resulting large set of 10 minute measurements allows us to search the data for correlations with variables such as elevation, parallactic angle, and time of day.

3. TELESCOPE AND RECEIVER SYSTEM

We used NASA's Deep Space Network (DSN) 34 m beam waveguide radio dish at DSS-13 in Goldstone, California. The receivers are readily accessible at the coudé focus, even while the antenna is in motion, and DSS-13 is the R & D antenna for the DSN, so the environment is well suited to debugging a new system and following up the small details essential in this type of project.

Figure 2 shows a block diagram of our receiver front end. The ultralow-noise amplifiers consist of a dual-cavity tunable maser, typically tuned (by adjusting the current in a

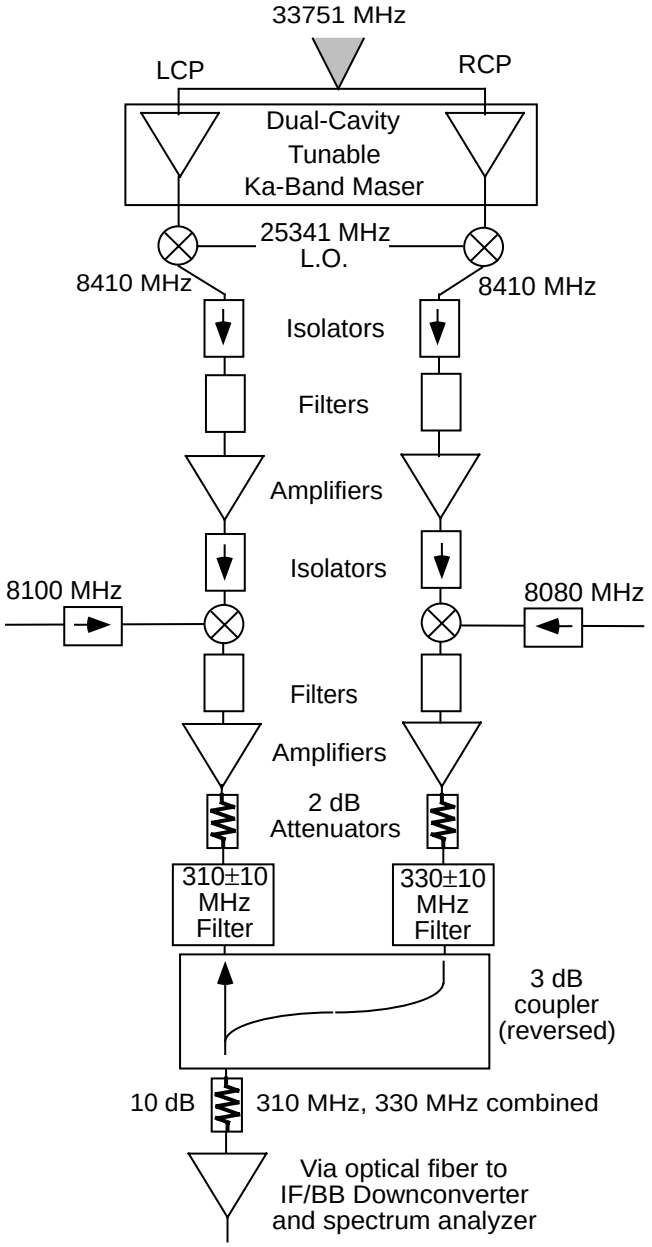

FIG. 2.—Block diagram of the dual-polarization Ka-band receiver system.

superconducting magnet) to 33,751 ± 100 MHz with a gain of 17 dB and a noise temperature of 5 K. Noise from the warm follow-on amplifiers added another 5 K to the system temperature, and atmosphere, antenna spillover, and cosmic background radiation added another 20 to 40 K, depending on weather, for a total system temperature that ranged from 30 to 50 K. Maser frequencies were tuned once per day during observation runs. The maser system is described in more detail by Shell et al. (1994) and was modified for our needs to include dual polarization. After initial amplification, the two signals (RCP and LCP) are further amplified with room-temperature HEMT amplifiers, mixed to *X*-band, mixed again to separate the spectral lines by precisely 20 MHz, and combined into a single bandpass for fiber-optic transmission and further mixing and filtering to a DC 40 MHz bandpass, as input to the wide band spectrum analyzer (WBSA). The WBSA is a 2,097,152 channel

digital spectrum analyzer with spectral resolution of 19.07 Hz per channel (Quirk et al. 1988). The WBSA and all the local oscillators were phase-locked with the DSN 5 MHz reference signal, to avoid any frequency drifts of RCP relative to LCP. To reduce the data storage required, WBSA channels were recorded only for the 8192 channels centered around the spectral line in each polarization. The spectra were periodically plotted and inspected to verify the absence of interfering signals.

4. DATA ANALYSIS AND RESULTS

We began observing L1498 with the new maser system when it became available in 1999 January and continued to observe it about once per week until 2000 March. After eliminating data affected by bad weather, procedural errors, and equipment failures, we have 209 measurements of L1498, each consisting of 10 minutes on source at R.A. (J2000) = $4^h10^m51^s.5$, decl. (J2000) = $25°10'5''.2$ (Fig. 1) and 10 minutes off source ($+1°$ in decl.).

We have analyzed the data in several ways, to check for potential systematic effects. For each measurement, we separately produce LCP and RCP spectra by calculating (on-off)/off and correcting for Doppler shifts due to the Earth's motion. Summing all the spectra (including both LCP and RCP), we fit the resulting spectrum to a Gaussian line shape, finding the amplitude, A, center frequency, v_0, and line width, σ, for which $A \exp[-(v-v_0)^2/\sigma^2]$ best fits the power as a function of frequency, v. We find the width to be $\sigma = 105$ m s^{-1}, as shown in Figure 3. Using this width, the LCP and RCP spectra for each individual measurement are fitted to Gaussian line shapes with unknown amplitude and center frequency, as well as to separate linear baselines. The signal-to-noise ratio (SNR) is estimated from the amplitude of the fitted line shape and the rms of the residuals. The frequency shift for each measurement is then the difference between the LCP and RCP center frequencies. The measurements are summarized in Table 1. Weighting by the square of the SNR and combining the results of all 209 measurements, the RCP spectral line is 34 ± 22 Hz (0.30 ± 0.20 m s^{-1}) lower in frequency than the LCP spectral line. The Zeeman splitting for the 33.751 GHz line of CCS is 0.702 Hz μG^{-1}, or 0.00624 m s^{-1} μG^{-1} (Shinnaga & Yamamoto 2000), so the line-of-sight component of the magnetic field is 48 ± 31 μG. As cross-checks, we have also separately averaged together all the LCP and RCP spectra and looked for a frequency shift by examining the cross-correlation and the RCP-LCP (Stokes V) difference (Fig. 3, *bottom right panel*). Results from all three calculation methods are consistent, with the maximum cross-correlation occurring at a shift of 0.17 m s^{-1}, while the best fit from the RCP-LCP difference is 0.30 ± 0.20 m s^{-1}.

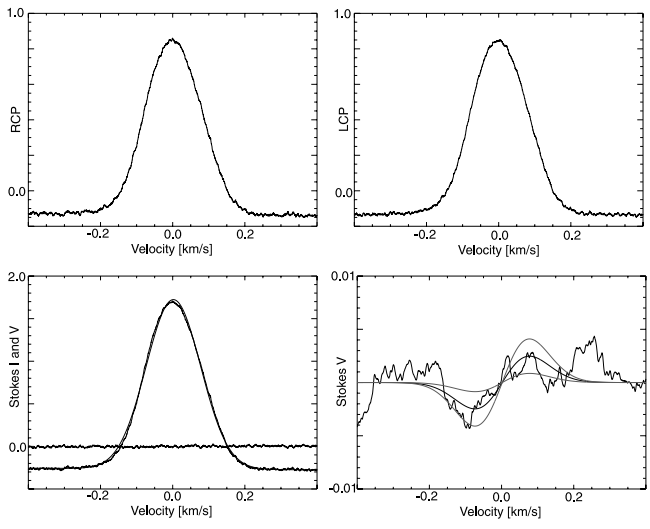

FIG. 3.—Spectral data, smoothed to 3 m s^{-1} resolution for display purposes. (*Top left*) RCP spectrum. (*Top right*) LCP spectrum. (*Bottom left*) Sum and difference of LCP and RCP spectra. The Gaussian line shape shown has a width $\sigma = 105$ m s^{-1}. (*Bottom right*) The difference of LCP and RCP spectra, smoothed to 105 m s^{-1}, with a linear baseline removed. The model shown is the difference of Gaussian line shapes centered at different frequencies, with the frequency shift chosen by minimizing χ^2. We also show the ± 1 σ variations of the model in the outer lines surrounding the fit.

TABLE 1

OBSERVATIONS

Year	Day	Zeeman Splitting (m s^{-1})	Number of On/off Pairs	Number Rejected
1999...	077	-2.11 ± 1.18	6	0
	082	-0.46 ± 0.78	15	0
	089	0.06 ± 0.92	11	0
	090	1.74 ± 1.51	9	0
	091	-1.32 ± 0.58	16	2
	095	0.35 ± 0.43	28	3
	098	-0.49 ± 0.94	9	0
	102	0.25 ± 0.80	23	3
	103	-0.80 ± 0.89	9	0
	105	-1.17 ± 0.776	11	0
	106	0.05 ± 1.28	8	0
	158	-4.93 ± 1.96	3	0
	165	-0.69 ± 0.85	19	1
2000...	005	1.23 ± 0.94	21	2
	027	0.88 ± 0.91	24	3
	033	-1.88 ± 2.85	3	0
	105	-1.44 ± 1.86	15	7

NOTES.—Each on/off pair corresponds to 9 minutes on source and 9 minutes off source, plus 1 minute at each position spent repointing and allowing the telescope to settle. The Zeeman splitting given for each day is the weighted sum of all valid on/off pairs for that day. We rejected 21 (of 230) on/off pairs with low SNR (typically) because of bad weather. An approximately equal amount of observing time was spent establishing the velocity gradient and measuring the RCP/LCP pointing difference (Fig. 6).

While we have designed the measurement to minimize or eliminate all known sources of systematic error, it is prudent to examine the data in search of any errors we may have failed to prevent. To look for possible systematic effects that might masquerade as Zeeman splitting, we have binned and plotted the 209 individual measurements in a variety of ways, as shown in Figure 4. In using such plots to derive limits on potential systematic errors, we must of course accept more noise than when averaging the entire data set into a single answer. By the same token, any systematic errors induced would be partly washed out by the fact that our full data set averages over a range of the controlling parameter. Here we discuss a few of the potential sources of error.

1. A fixed (relative to the telescope) difference in pointing between RCP and LCP would result in an error proportional to a sine wave in parallactic angle. Because our observation time is not evenly distributed in parallactic angle, any such effect would average out imperfectly, leaving a residual error. As shown in Figure 4*a*, we see no

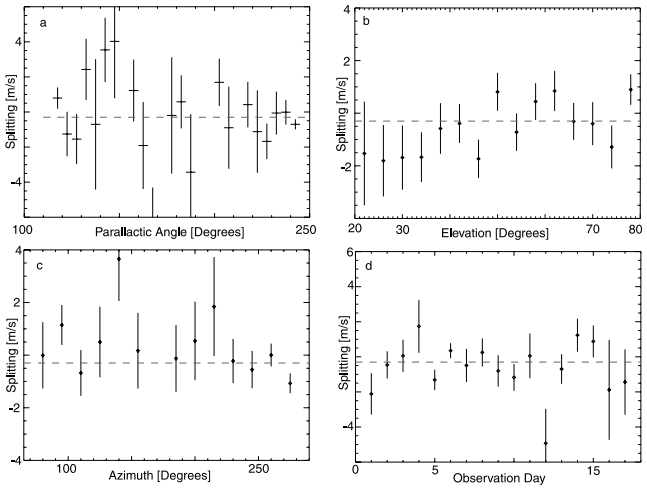

FIG. 4.—Distribution of observed Zeeman splitting (in meters per second) in individual measurements as a function of: (*a*) Parallactic angle, in 5° bins. There are comparatively few measurements at intermediate parallactic angle, so the error bars are larger in the middle of the plot. A constant difference in pointing between LCP and RCP would produce a sine wave with a 360° period. The dashed line represents the weighted average of all measurements. (*b*) Elevation, in 4° bins. The systematic variation in noise is due to the effect of antenna efficiency variation on the system temperature. (*c*) Azimuth, in 15° bins. (*d*) Chronological order, in 1 day bins.

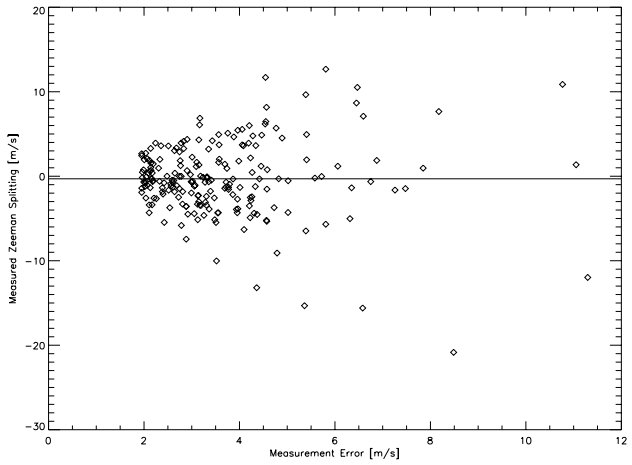

FIG. 5.—Observed frequency shift vs. nominal measurement error. Note that the data appear to be distributed about a single mean (-0.3 m s^{-1}), with high-SNR measurements showing less scatter than low-SNR measurements.

variation with parallactic angle and no evidence for such an effect, but from Figure 4*a* alone we cannot rule out an effect as large as 2 m s^{-1} (300 μG), which could leave a significant residual when averaged over the 130° range in observed parallactic angle. This potential systematic error is discussed further below.

2. Polarization-dependent effects caused by gravitational deformation of the telescope would be expected to vary with elevation, and, as shown in Figure 4*b*, no elevation dependence is evident at about the 1 m s^{-1} (150 μG) level. Without knowing the functional form of this hypothetical effect, we cannot use the plot to quantitatively establish an upper bound for its impact on the final result. Nonetheless, the lack of any visible effect is a useful cross-check.

3. Spillover effects or problems associated with the beam-waveguide optics could manifest themselves as an azimuth dependence, but again we see no such variation (Fig. 4*c*) at about the 1 m s^{-1} level.

4. We also found no evidence for dependence on other variables, such as day of observation (Fig. 4*d*) and the SNR (Fig. 5), which could result from polarization-dependent effects due to receiver variation, weather, or low-level RFI.

The possibility of RCP/LCP pointing differences is particularly important, because beam-waveguide dishes are known to have a polarization-dependent squint (Houshmand 1991). We have measured the difference in pointing between the LCP and RCP channels, using Venus, Mars, and 3C 273 as point sources and fitting the beam shape as Gaussian. As evidenced by the results plotted in Figure 6, the pointing difference is less than 0°.001 and is not constant. The points in Figure 6 show scatter as a result of noise in the individual measurements, but they clearly exhibit a systematic variation as the telescope tracks the test sources in azimuth and elevation. As shown in Figure 1, we chose to observe L1498 at the central core location, where the velocity gradient is very small. We have mapped the surrounding velocity structure in a 3 × 3 grid with spacing 0°.004 and used the beam size (~0°.018) to estimate the maximum velocity gradient possible over a 0°.001 span at the observed location. Including the possible effect of the spatial gradient in the Doppler correction due to Earth's motion, the largest possible velocity gradient (as seen in our beam) is 0.2 m s^{-1} per 0°.001. The actual error caused by pointing differences is smaller, because the pointing offset does not align with any single direction on the sky, but varies as the telescope tracks the source in azimuth and elevation, so that it must partly average out over the full

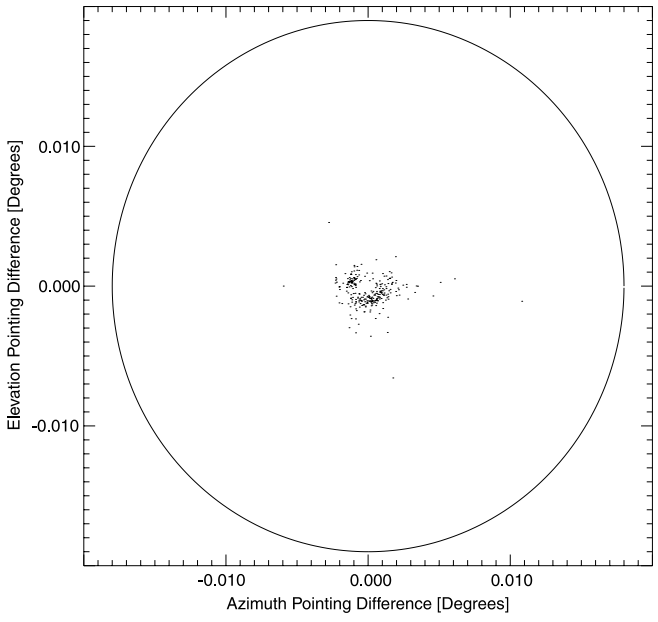

FIG. 6.—Measured pointing difference between LCP and RCP for NASA's DSN DSS-13 34 m antenna, in azimuth/elevation coordinates. The ellipse represents the beam shape. The half-power beamwidth is 0°.018 in azimuth and 0°.019 in elevation. The data show random noise from the individual measurement errors superposed on a systematic variation as the telescope tracks. The systematic pointing difference averages to nearly 0 but can be as large as 0°.001 at some combinations of azimuth and elevation. The possible consequences of such an effect are discussed in the text.

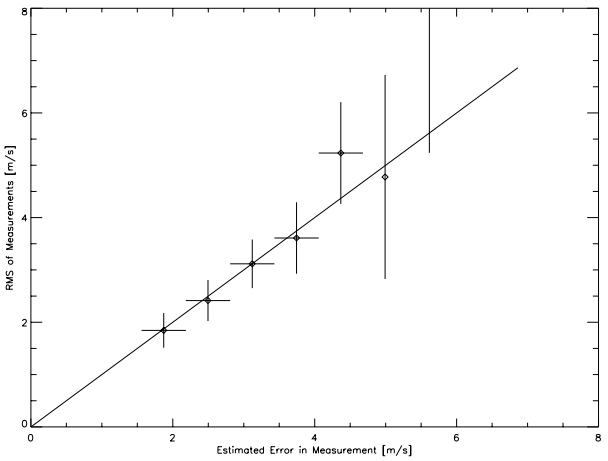

FIG. 7.—Observed scatter in Zeeman-splitting measurements vs. nominal error based on the signal-to-noise ratio. The line indicates the relationship expected if the error estimate is accurate.

set of observations. We estimate that the error caused by pointing differences is less than 0.1 m s^{-1}. We have also examined the data for correlations between observed Zeeman splitting and parallactic angle, time of day, time of year, azimuth, and elevation, and we find no evidence for contamination by a polarization-dependent beam squint effect.

In combining the 209 measurements, we have estimated the SNR by comparing the line strength to the rms of the residual after subtracting the spectral line and baseline. We have used this SNR both for weighting purposes and to estimate the uncertainty in our result, so it is important to verify its validity. With our data set ordered from smallest to largest estimated error, the scatter in the measurements gives us an independent check on the uncertainty and hence on the SNR estimate. As shown in Figure 7, the scatter is consistent with our estimated uncertainty.

5. DISCUSSION

Our formal result of 48 ± 31 μG implies a 95% confidence level upper limit of 100 μG on the line-of-sight component of the magnetic field strength in the core of L1498. Various estimates have been made of the minimum magnetic field needed to support a cold molecular cloud (Mouschovias & Spitzer 1976; Tomisaka, Ikeuchi, & Nakamura 1988, and references therein). Following Crutcher (1999), we take the critical field strength to be about $N(H_2)/(10^{20}\ \mathrm{cm}^{-2})$ μG. At our observing location in L1498, the hydrogen column density is $N(H_2) \simeq 10^{22}$ cm^{-2} (Willacy et al. 1998), implying a critical field strength of about 100 μG, within the range implied by our measurement. The magnetic field strength also has implications for the possible presence of MHD waves. The thermal line width for CCS at the ~ 10 K temperature of the core is only $\sigma_{\mathrm{th}} \simeq 44$ m s^{-1}, while the measured width is $\sigma = 105$ m s^{-1}, requiring a nonthermal width of $\sigma_{\mathrm{NT}} = (\sigma^2 - \sigma^2{}_{\mathrm{th}})^{1/2} \simeq 95$ m s^{-1}. If we attribute this to random motions at the Alfvén velocity and use the hydrogen density of 10^4 cm^{-3} estimated for this part of the core, we derive a magnetic field of 73 μG, consistent with our measurement.

As one can well appreciate, 70 hr of observing time is substantial for a single astronomical observation, especially because considerable additional time was spent on characterizing the system, plus time spent observing under conditions for which the data cannot be used. Thus, it is important to address the issue of whether measurements of the CCS line at 33 GHz can be an important probe of magnetic field strengths in clouds at the 50 μG level or lower, typical of what might be expected in the pre-protostellar core stage. To date, our measured sensitivity continues to improve as the square root of the time, so we might expect to reduce the error bar to 22 μG with another 70 hr of observation (and corresponding observations to improve our knowledge of the pointing offset and the velocity structure of L1498). As we are nearly at the sensitivity limits of receiver-antenna systems at this frequency, we are not likely to improve on this error bar by more than a factor of 1.5. A more promising approach is to perform similar measurements with the lower-frequency transitions of CCS. The lines at 22 and 11 GHz have been detected (Fiebig 1990), and at the relevant temperatures (~ 10 K), densities [$n(H_2) \sim 10^4$–10^5 cm^{-3}], and fractional abundances (Wolkovitch et al. 1997) they have very similar intensities to the 33 GHz line. However, the ratio of Zeeman splitting to line width improves linearly with frequency, and receiver systems and atmospheric emission will be better at 22 GHz (the $J_N = 2_1$–1_0 transition) and much better at 11 GHz (the $J_N = 1_0$–0_1 transition). For example, with currently available technology, an 11 GHz receiver at DSS-13 could be expected to achieve a system temperature of 20 K (compared with 40K at 33 GHz). One could also greatly reduce the need for off-source observations by using frequency switching, and the antenna efficiency is better at 11 GHz than at 33 GHz, resulting in an expected sensitivity of ± 10 μG in 20 hr of observation of L1498. In conclusion, we have shown that CCS Zeeman splitting is a promising approach to measuring the magnetic field in cloud cores with the antennas and receiver systems available today.

We greatly appreciate the advice and assistance of Jim Shell, Bob Clauss, and Doug Hofhine, which made possible the use of the dual-polarization maser. This work would not have been possible without the invaluable support of the personnel of DSS-13, the DSN's Research and Development station. We would also like to thank H. Pickett for advice concerning CCS properties. We thank the referee for helpful comments, which have resulted in improvements. This research was carried out at the Jet Propulsion Laboratory, California Institute of Technology, under a contract with the National Aeronautics and Space Administration.

REFERENCES

Crutcher, R. M. 1999, ApJ, 520, 706
Crutcher, R. M., & Troland, T. H. 2000, ApJ, 537, L139
Fiebig, D. 1990, Ph.D. thesis, Univ. Bonn
Houshmand, B. 1991, IEEE Trans. Antennas & Propagat., 39, 262
Kuiper, T. B. H., Langer, W. D., & Velusamy, T. 1996, ApJ, 468, 761
Mouschovias, T. C., & Spitzer, L., Jr. 1976, ApJ, 210, 326
Quirk, M. D., Wilck, H. F., Garyantes, M. F., & Grimm, M. J. 1988, IEEE Trans. Acoustics, Speech, & Signal Processing, 36, 1854
Shell, J., et al. 1994, Proc. IEEE, 82, 806
Shinnaga, H., & Yamamoto, S. 2000, ApJ, 544, 330
Tomisaka, K., Ikeuchi, S., & Nakamura, T. 1988, ApJ, 335, 239
Willacy, K., Langer, W. D., & Velusamy, T. 1998, ApJ, 507, L171
Wolkovitch, D., Langer, W. D., Goldsmith, P., & Heyer, M. 1997, ApJ, 477, 241